Opto-Electronics Review

journal homepage: https://journals.pan.pl/opelre



Use of graphene oxide as an active layer on a tapered fibre for detection of volatile liquid vapours: ammonium hydroxide, trimethyl phosphate, and 1,4-thioxane

Julian Krawczyk[1], Joanna Korec-Kosturek[2], Rafał Kosturek[2], Iwona Jakubowska[2], Anna Pakuła[1], Małgorzata Djas[3,4], Krystian Kowiorski[4], Karol A. Stasiewicz[2*]

[1] Institute of Micromechanics and Photonics, Warsaw University of Technology, ul. św. Andrzeja Boboli 8, 02-525 Warsaw, Poland
[2] Institute of Applied Physics, Military University of Technology, ul. gen. Sylwestra Kaliskiego 2, 00-908 Warsaw, Poland
[3] Faculty of Chemical and Process Engineering, Warsaw University of Technology, ul. Waryńskiego 1, 00-645, Warsaw, Poland
[4] Department of Functional Materials, Łukasiewicz Research Network – Institute of Microelectronics and Photonics, al. Lotników 32/46, 02-668 Warsaw, Poland

Article info

Article history:
Received 03 Feb. 2025
Received in revised 26 Feb. 2025
Accepted 26 Feb. 2025
Available on-line 02 Apr. 2025

Keywords:
G-Flake graphene oxide layer;
vapour detection;
in-line optical fibre sensors;
volatile liquid sensors;
gas sensors;
optical fibre technology.

Abstract

This paper investigates the application of a G-Flake graphene oxide (GO) layer as an innovative coating material for optical fibre tapers, enhancing the sensor sensitivity to various volatile liquid vapours. The results confirm that this combination is effective because the formation of a monolayer of adsorbed gas alters light propagation in the tapered optical fibre. These changes are detectable across a broad wavelength spectrum, ranging from visible to infrared. In this study, three volatile liquids – trimethyl phosphate (TMP), 1,4-thioxane (THX), and ammonium hydroxide (NH_4OH) – were tested using pure THX and TMP without dilution, while NH4OH was applied as a 25% solution. The gases used in the research simulate chemical warfare agents, such as sulphur mustard and sarin. The authors used the differential method to analyse the results, which revealed the formation of characteristic peak pairs around a wavelength of 795 nm. The peak heights and the distance between them varied over time in response to exposure to the selected vapours. Additionally, the amplitude of the transmitted power changes linearly in the first 30–45 min, with the highest power change rate observed for TMP (0.026 dBm/min at 789.2 nm). The greatest contrast between maximum and minimum power levels was observed for TMP, reaching 4.45 dBm. An approach was presented that demonstrates how a tapered fibre covered with GO can be used as the basis for developing a low-cost gas and vapour sensor.

1. Introduction

Fibre optic sensor technology plays a growing role in many fields, such as healthcare [1], environmental monitoring [2], and industry [3]. The unique qualities of optical fibres – insensitivity to electromagnetic interference, flexibility and small weight, high sensitivity to selected factors for special fibres, and the possibility to achieve quick response times in measurement systems make them incredibly versatile. These features find applications in everything from telecommunications to cutting-edge optoelectronic devices. One of their most widespread uses is in the creation of optical sensors, which are highly effective tools for measuring a variety of chemical and physical parameters, including refractive index [4], temperature [5], pressure [6], vibrations [7], and even the presence of gases or chemicals [8, 9]. There exist different kinds of fibre sensors which can use fibre as an element of incoming and outgoing light to the measuring system, detecting changes using a unique internal structure or using a change in fibre geometries, such as side-polished fibres, U-shaped fibres, or tapered optical fibres. Two of the last sensor systems mentioned above, often called in-line measurement systems, are systems in which light propagates inside a fibre without being derived and interacting with the tested factor. Fibre

*Corresponding author at: karol.stasiewicz@wat.edu.pl

https://doi.org/10.24425/opelre.2025.154305
1896-3757/ Association of Polish Electrical Engineers (SEP) and Polish Academic of Sciences (PAS). Published by PAS
© 2025 The Author(s). This is an open access article under the CC BY license (http://creativecommons.org/licenses/by/4.0/).

tapers are one of the most straightforward configurations. Their growing interest in experimental measurements and simulations is due to their high sensitivity and low insertion loss, versatile use, and the possibility of combining them with additional materials [10–12]. Among the fabricating methods, the common techniques include chemical etching, polishing, and the heat-and-pull method. In this article, the heat-and-pull technique is used, which involves heating the fibre to its softening point and simultaneously pulling it from both ends to achieve a fibre with a partially reduced diameter. This method offers advantages like precise control over the taper geometry and the adiabatic shape which responds to minimal internal losses. The in-line sensors based on tapered optical fibres are often combined with functional materials as their coatings increase or enable the detection of chosen factors. The most interesting materials used as new coatings should be liquid crystals [13], alkanes [14], polymers [15], metals [16], and advanced materials like graphene and graphene oxide (GO) [17, 18]. GO has emerged as a revolutionary material in sensing technology due to its unique properties like high surface reactivity, electrical conductivity, large surface area, and excellent mechanical strength [19–21]. Integrating GO layers with tapered optical fibre sensors can further improve their capabilities, enabling detection of different chemical and biological analytes [22–24]. The special design, including a functional group on GO, allows for an easy attachment of specific gases, like CO, NO, NH_3, and SO_2 [25], liquids, including ethanol, acetone, isopropanol [26], and biomolecules, especially DNA and proteins [27].

Recent advancements have demonstrated that GO-coated optical fibres can achieve high sensitivity and selectivity. In 2020, Yang *et al*. reported a very sensitive glucose sensor. The results indicate that the sensor model developed in this study demonstrates excellent sensitivity in detecting glucose levels in the human body. It offers a sensitivity of 1.06 nm/mM within the linear detection range from 0 mM to 11 mM, with an autocorrelation accuracy of 0.9386 [28]. In 2023, the group of Alkhabet *et al.* presented a GO-based gas detector. A newly developed sensor demonstrated a strong sensitivity to hydrogen (H_2) concentration variations at 100 °C. For a 2.00% H_2 level, the response time was measured at 2 min, while the recovery time was 11 min.

Additionally, the optical fibre sensor showed remarkable selectivity and stability for detecting H_2 gas, even when exposed to other gases like ammonia (NH_3) and methane (CH_4) [29]. In 2021, Qi *et al*. reported a chalcogenide-etched tapered fibre-based sensor functionalized with a GO film [30]. The GO-coated sensor exhibited enhanced detection capabilities with sensitivities increasing to 4.5091 a.u./mg·mL^{-1} for liquids and 0.4812 a.u./vol.% for gases – improvements of 69% and 74%, respectively, compared to the uncoated version.

In this study, tapered optical fibres were created as the core components for sensor applications using the low-pressure flame method. The manufacturing process involves heating fibres to a temperature between 1100–1200 °C, which is their softening point, and simultaneously pulling the fibres from both ends to reduce their diameter and form a taper with minimal internal losses. This research was set out to investigate how tapered optical fibres, combined with a functional material like GO, could be used to build sensors for liquid vapours.

Numerous other studies confirm the effectiveness of combining tapered optical fibres with GO layers for detecting gases and their vapours [31, 32]. The authors' previous findings revealed that the GO layer altered the boundary conditions influencing light propagation within the fibre as a result of the physical adsorption of chemicals. This study focused on investigating the changes in light propagation properties of a tapered optical fibre coated with a GO layer exposed to various liquids and their vapours, such as ammonium hydroxide (NH_4OH), trimethyl phosphate (TMP), and 1,4-thioxane (THX). The gases used in the research are simulants of chemical warfare agents such as sulphur mustard and sarin which are among the paralytic-convulsive agents and posing significant health hazards. Hence, the research aimed to investigate the possibilities of constructing simple in-line fibre optic sensors and the development of a new, low-cost solution for detecting gases and volatiles. The constructed measurement system allows only qualitative, not quantitative, analysis of adsorbed substances. This limitation arises because air is in the chamber and the liquids inside are left to evaporate freely. Additionally, the evaporating liquids can adsorb onto the chamber walls, making it impossible to determine a specific concentration of the substances.

Used technology is easy to use and has several advantages, including low cost, fast manufacturing, and high repeatability. Hence, the obtained device has the potential for detecting the presence of selected substances, paving the way for the development of precise, modern gas sensors with potential applications in environmental monitoring.

2. Materials and methodology

2.1. Materials for the GO devices

The proposed high-sensitivity sensors use a property of the modified optical fibre through a tapering process which allows to directly influence the propagating beam in the structure. An optical phenomenon enabling interaction of optical beams with other materials is connected with the evanescence wave [33] and deep penetration [34] of this wave which can be increased during tapering. Many articles widely described the tapering process [35, 36]. The fibre optic taper element technology (FOTET) system for taper manufacturing uses a low-pressure gas burner with propane-butane and oxygen mixture. When the fibre reaches the required temperature, it is simultaneously stretched in opposite directions to achieve the desired tapered length directly determining the final diameter. The authors' previous publication has a detailed description of the manufacturing process and system [36]. Based on the experience and experimental selection of the fibre diameter for which the leaking wave best interacts with the tested materials, a taper with a total extension length of 22.05 ± 0.15 mm was used for the research work. This extension length corresponds to a specific area diameter of 10.0 ± 0.5 μm and internal losses below 0.25 dB at 1550 nm, which meets the conditions of adiabaticity [37]. A standard SMF28 from Corning Company (Corning, NY, USA) for the telecommunication range was used as a fibre.

Using a modified Hummers method, GO (G-Flake) was produced at the Łukasiewicz Research Network – Institute of Microelectronics and Photonics. This is a chemical method for obtaining GO [38, 39]. Graphite flakes of 100 to 120 µm (Asbury Carbons, USA) were used as a precursor. A modified Hummers method obtained GO flakes of 6 to 14 µm.

In this article, the authors investigated three volatile compounds – TMP, THX, and NH_4OH – using pure THX and TMP without dilution, while NH_4OH was applied as a 25% aqueous solution. In this study, the most important property of these compounds was their respective vapour pressure. Vapour pressure is one of the properties that characterise volatility. Vapour pressure is related to the ability to evaporate. Liquids with high vapour pressure evaporate easily, while those with low vapour pressure evaporate slowly and not completely. It is presented as follows: 25% solution of NH_4OH – 483 hPa in 20 °C, pure THX – 7.53 hPa in 25 °C, and pure TMP is 1.133 hPa in 25 °C.

2.2. *Experiment*

The experimental setup shown in Fig. 1 for broad spectrum measurements included, as a light source, a SuperK EXTREME Supercontinuum from NKT Photonics working in the optical range of 350 nm –2400 nm, coupled to a tapered optical fibre covered with GO. The spectral analysis was performed using an optical spectrum analyser (OSA) AQ6373 (YOKOGAWA, Tokyo, Japan) working in the range of 350 nm–1200 nm.

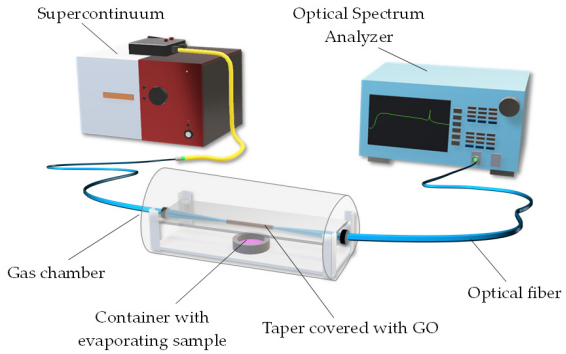


Fig. 1. A setup for measurement in a broad-spectrum, containing supercontinuum and optical spectrum analyzer.

All measurements were conducted on a passive, isolated optical table at room temperature between 20 and 21 °C, with conditions maintained using an air conditioner and atmospheric pressure of approximately 1000 hPa. The samples were tested several times to check the repeatability of the provided measurements. Only minor differences in power levels were observed between samples, resulting from losses introduced during the tapering process and from welding the fibre connectors to the tapers. A 100 µL volume container was used to analyse all the liquid vapours. The testing chamber, designed at the authors' institute, has a total volume of 0.8 m^3 and the analysed sample was directly above the container containing the liquid. Hence, in the next paragraph, typical obtained results are presented for a tapered optical fibre covered with GO and exposed to vapours of various liquids: NH_4OH, THX, and TMP.

3. Results and discussion

In this study section, the authors examined how the adsorption of three different vapours affects light propagation. The gas adsorption process on the graphene layer is based on two main mechanisms: physical adsorption resulting from van der Waals interactions and chemical adsorption related to forming C-X bonds. The so-called active spots of the sorbent can adsorb only one molecule of the target gas, forming a monomolecular layer on the surface. Over time, as adsorption progresses, the sorptive surface becomes saturated by which the sensor does not respond to the presence of additional gas. A detailed description of the adsorption process has been provided in our previous publication [40].

It should be noted that, unlike in the authors' previous article, volatile liquids were used. Therefore, the response time of the created sensor is limited by the evaporation rate. Hence, a single measurement was conducted in 120 min. Each time, 100 µl of liquid was added to the vessel which was positioned beneath the taper. To demonstrate the actual impact of the vapours and the time increase of new layers due to adsorption, the authors will present differences between the characteristics obtained for tapers with adsorbed gases and the reference values before the evaporation process. The spectra measurements were conducted in the 700–1200 nm wavelength range, where the highest change was observed and was able to be described. Due to the use of a standard single-mode optical fibre in the telecommunications wavelength range and because the taper profile is insufficient to cut off higher-order modes, the taper exhibits multimode propagation in this wavelength range. Due to the large number of peaks in the full spectrum used in this measurement, which are the effects of intermodal interference, the specific regions were selected for further analysis where the most significant changes were observed. Each time the first measurement (0 min) was taken without the tested substance, the sensor was exposed to vapour and the optical characteristics were recorded sequentially at different exposure time intervals. The results obtained for all samples are presented in the same manner. Firstly, the authors focus on the full spectrum overview, and then, for the selected wavelengths, the power levels concerning time of exposure to vapours are discussed. The final analysis involves measuring the change in the distance between characteristic peaks in the 750–850 nm range.

The first analysed volatile liquid was NH_4OH. Figure 2 shows the spectral characteristics of a taper optical fibre (TOF) exposed to its vapour. Above the wavelength range of 700 and 750 nm, the power level does not show significant deviations from the reference measurement. The power transmission differences start to increase around 750 nm. In the 920 to 1000 nm range, there is again a region where the power level remains similar to the reference. However, as observed beyond 1000 nm, there is a significant change in transmission characteristics and disappearance of multimodal interference. Peaks are no longer visible and the power level decreases as the exposure time to the ammonium hydroxide solution increases. The graph shows a difference between the maximum and minimum power levels after 120 min of exposure, which is about 3.22 dBm.

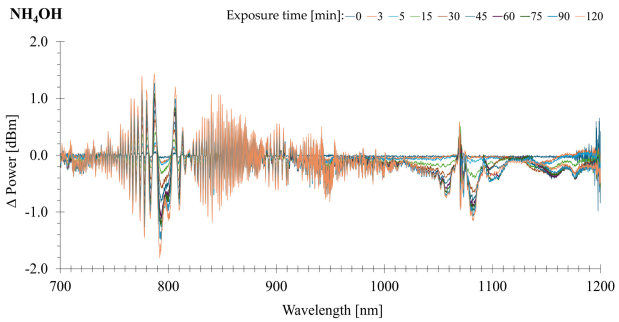


Fig. 2. Changes in spectral characteristics of TOF with a GO layer during exposure to evaporating NH_4OH.

As observed, the spectral characteristics change as the liquid evaporates and adsorbs onto the graphene. Peaks emerge and become more pronounced with longer exposure to the vapours, though noticeable changes can be seen after just 3 min. To illustrate the time-dependent changes, several wavelengths from the full measurement range were selected. The relationship between power level and exposure time to NH_4OH vapour is shown in Fig. 3. Within the 750 to 1000 nm range, the most significant and linear power changes occur within the first 30 min, with a correlation coefficient (R^2) exceeding 0.99. For the selected wavelengths of 1060 nm and 1159.4 nm, the rate of power change begins to decrease after 45 min of exposure. Stabilization and no further change in power are observed after 90 min of exposure.

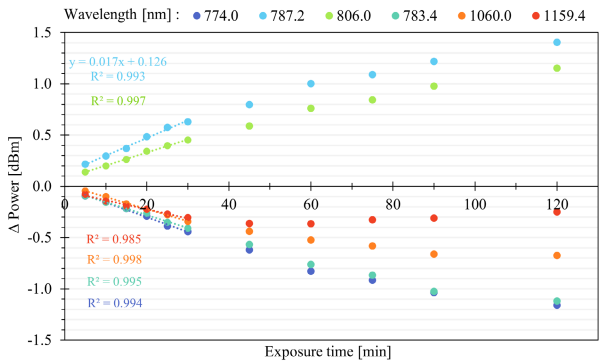


Fig. 3. Power changes for selected wavelengths during the exposure of TOF with a GO layer to evaporating NH_4OH.

Among all chosen wavelengths, the highest power change rate is observed at 877 nm, with a value of 0.017 dBm/min. The lowest values are found in the near-infrared (NIR) region, where the rate is approximately 0.01 dBm/min. The noticeable slowdown in power level changes is attributed to the deposition of vapour particles from the selected chemical compounds onto the GO layer, leading to the saturation of the graphene oxide layer.

In the full spectrum, characteristic peaks around 800 nm can be observed which move away from each other with an increasing exposure time to NH_4OH vapour. To illustrate this phenomenon, six of these peaks were selected and grouped into pairs (see Fig. 4) with calculated distances between them.

During a 120 min exposure to NH_4OH vapour, the distance between the first pair of peaks increased by 2.0 nm

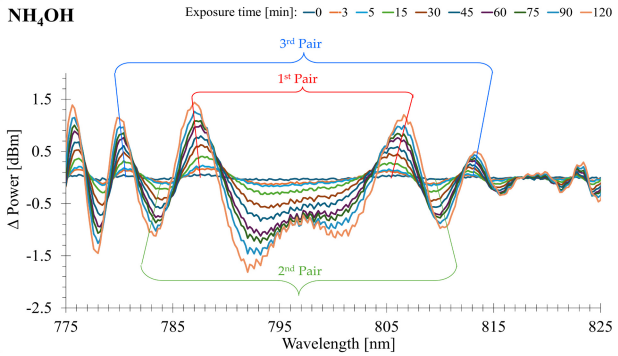


Fig. 4. Characteristic peaks shift *vs.* exposure time to evaporating NH_4OH.

and by 2.4 nm for the second pair. The third pair of peaks shifted their maxima by 1.6 nm compared to their positions at 5 min. The highest rate of change was observed during the first 45 min of exposure, after which no significant increase in peak distances was noted. As observed, the distance between the peaks increases over time, following a significant logarithmic trend with an R^2 value higher than 0.93 (see Fig. 5).

The second investigated liquid was TMP, with measurement results in Figs. 6–9. Compared to the spectra obtained for NH_4OH, the difference between the maximum and minimum power levels after a 120 min exposure to TMP was around 4.45 dBm. As can be seen, compared to NH_4OH, significant changes in the case of TMP vapour occur only after a 15 min exposure to the substance due to the much higher evaporation temperature. Figure 6 presents the complete spectral characteristics of the TMP liquid vapours.

Figure 7 shows the power change for six wavelengths in the 775–1079 nm range. The power increases with increasing exposure time for shorter wavelengths from 775 to 803.8 nm.

However, after 60 min, the rate of change decreases, and after 75 min, the power level stabilizes. The power change is linear in the first 30 min of the exposure time; the obtained R^2 is over 0.99 in most cases. For the more extended spectral range, for wavelengths 1059.6 nm and 1079 nm, the power change graph shows fewer minor differences than shorter wavelengths and signal stabilization occurs just after 30 min.

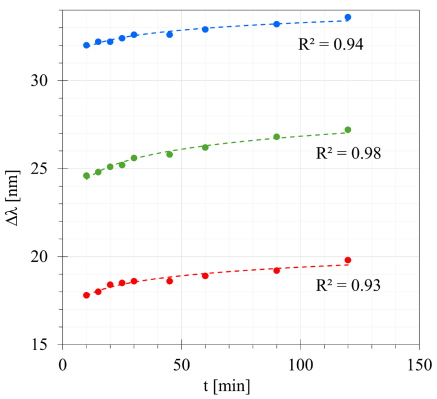


Fig. 5. Exposure time to evaporating NH_4OH.

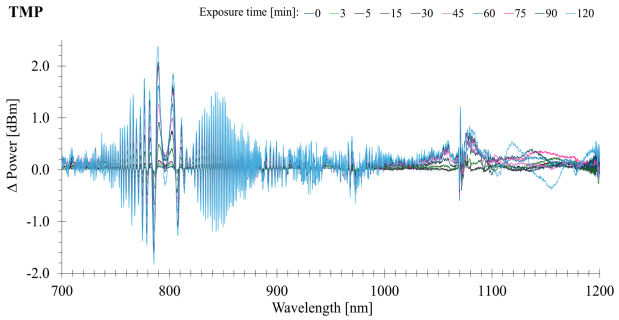


Fig. 6. Spectral characteristics of TOF with a GO layer during TMP exposition.

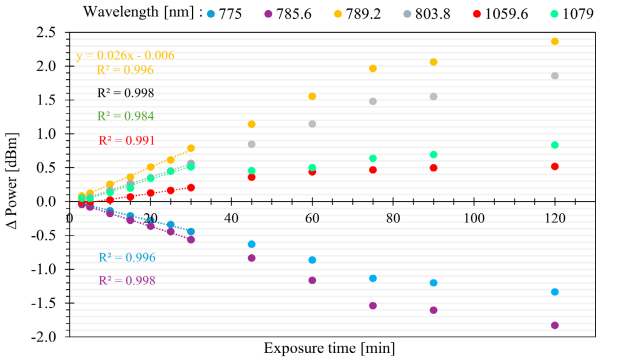


Fig. 7. Power changes for selected wavelengths as a function of exposure time to TMP vapours.

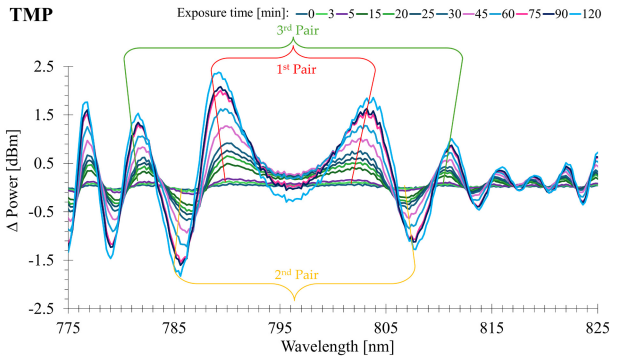


Fig. 8. Characteristic peaks shift *vs*. exposure time to TMP vapours.

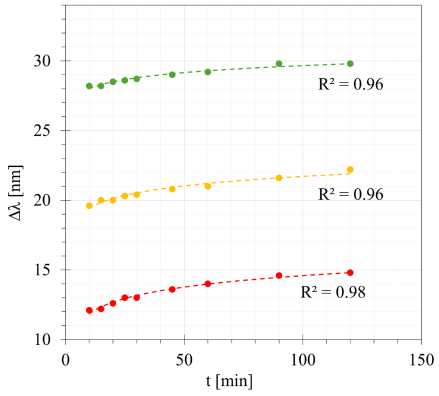


Fig. 9. Exposure time to TMP vapours.

Furthermore, for longer wavelengths, signal fluctuations are noticeable. In this case, the highest value of the power rate change is observed, which is 0.026 dBm/min for 789.2 nm. The rate of change in the NIR region is comparable with the results obtained for NH_4OH and is 0.01 dBm/min.

Similar to the measurements with NH_4OH, a slight shift in peaks was observed, most evident in the 750–850 nm range. The distances between these peaks were calculated and presented in Fig. 8.

As can be observed, the maximum shift occurs for the first and second pair of peaks, the distance between which increased by about 2.6 nm after 120 min and this shift is higher than in the case of NH_4OH. For the given third pair, the distance increased by 1.6 nm after 90 min of exposure to TMP, with no further changes over time.

As for the past liquid vapours, the calculated distance between the peaks increases over time, following a significant logarithmic trend with an R^2 value greater than 0.96 (see Fig. 9).

The last tested liquid was THX and the obtained results are presented in Figs. 10–13. In this case, the maximum difference between the highest and lowest power levels after the 120 min exposure is the smallest, amounting to nearly 3.0 dBm. Similar to TMP, the first significant spectral changes can be observed after 15 min of exposure. Figure 10 presents the whole spectral characteristics.

Six wavelengths were selected for further analysis from the entire spectrum (see Fig. 11). As in previous cases, the power changes show linearity. Still, this linearity persists up to 45 min of exposure to THX. After this time, a sudden shift occurs. Moreover, compared to the previous compounds, the R^2 coefficient is lower for the analysed wavelengths, exceeding 0.99 in only two cases: 787 nm and 806 nm. The maximum power change rate is similar to NH_4OH, measured at 0.018 dBm/min.

In the case of a THX liquid vapour exposure, six peaks were selected and the measurement distances between them were calculated, showing the effect of adsorption on beam propagation. The results are presented in Fig. 12. As observed, the changes in distances between the selected characteristic peaks remain small (below 0.8 nm) for up to 30 min of TOF exposure. The total peak shift is the smallest among the tested substances, amounting to 2 nm for the first and second pairs of peaks and 0.8 nm for the third pair. Notably, the increasing distance between the peaks exhibits significant logarithmic changes with a high correlation coefficient exceeding 0.96.

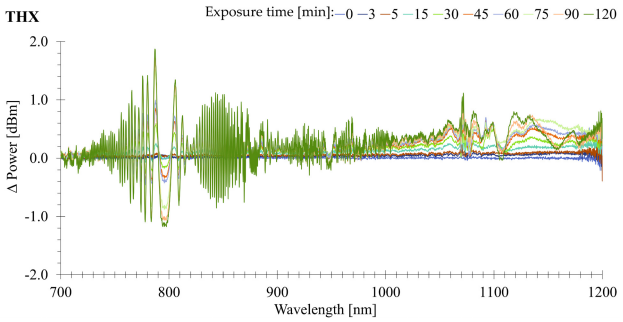


Fig. 10. Spectral characteristics of TOF with a GO layer during THX exposition.

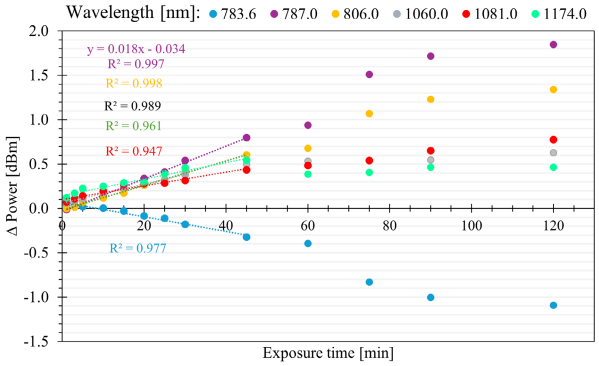


Fig. 11. Power changes for selected wavelengths during the exposure of TOF with a GO layer to THX gases and vapours.

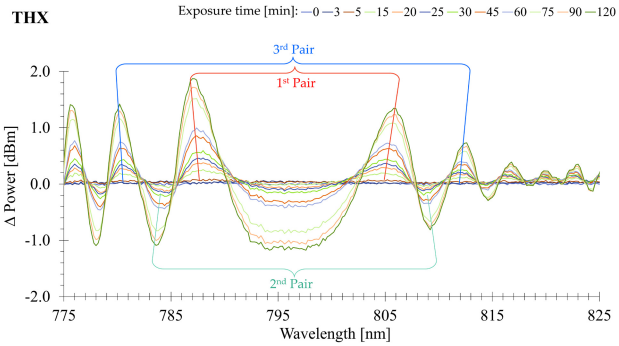


Fig. 12. Characteristic peaks shift *vs*. exposure time to THX vapours.

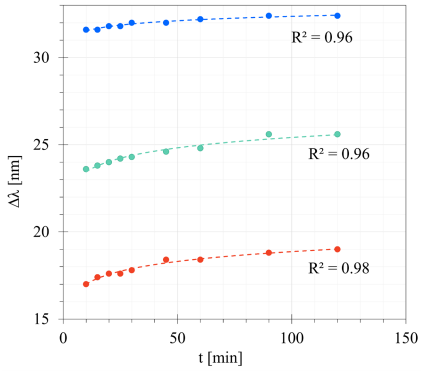


Fig. 13. Exposure time to THX vapours.

Figure 13 presents a logarithmic trend with an R^2 value higher than 0.96 for THX, which is correlated with TMP results.

As shown in the above results, the GO-layer sensor type allows the differentiation and detection of selected liquid vapours. For each measured liquid, the authors obtained characteristic peaks and wavelengths over a wide spectral range from which they can correctly identify them. Changes in the rate of vapour adsorption to the layer and the amplitude of the propagating beam, which depends on the material to be detected and, in particular, on the parameters of the new adsorption layer being formed, are both visible. The largest changes over the first 30 min are observed for TMP vapours, followed by THX, and the least dynamic are for NH_4OH. It should also be noted that the total change amplitude for 120 min is the lowest for NH_4OH. – less than 1.5 dBm and the highest for TMP – below 2.5 dBm.

4. Conclusions

The presented research on the possibilities of detecting various liquids and their vapours, such as NH_4OH, TMP, and THX in-line detector based on a TOF with a new GO layer as a signal-amplifying material, allows for the following conclusions.

A significant change in the power level for NH_4OH occurred within the first 5 min, while for others they appeared after a longer duration, which depended on the evaporation rate of the respective liquid. The peaks generated by intermodal interference differ in power amplitude depending on the type of adsorbed vapour. The highest contrast between maximum and minimum power levels was observed for TMP, reaching 4.45 dBm.

Shorter wavelengths in the range of 750–850 nm are the most sensitive to changes in boundary conditions due to vapour adsorption and exhibit the most significant spectral changes.

Power changes for NH_4OH and TMP remain linear for up to approximately 30 min, while for THX, this linearity extends up to 45 min. Such change is evidenced by a very high correlation coefficient, often exceeding 0.99. After these periods, a noticeable slowdown in the rate of power changes occurs eventually leading to signal stabilization due to the GO layer saturation. Furthermore, this phenomenon is more pronounced at longer wavelengths in the NIR range.

Pairs of characteristic peaks formed around a 795 nm wavelength move further apart with increasing exposure time to the given vapours and these changes follow a logarithmic trend.

In summary, coating the waist of the tapered fibre with a GO layer enables the effective detection of the presence of tested liquid vapours by amplifying high intermodal interference peaks and obtaining a characteristic spectrum. The changes in the spectrum, caused by the deposition of molecules on the GO layer, vary depending on the tested substance and become noticeable within just a few minutes. However, long-term studies are essential considering the evaporation time of the selected substances. Prolonged exposure enables assessing the sensor behaviour, such as changes in peak height and distance, and facilitates the differentiation between various gas vapours. The results and conclusions suggest that the optical fibre element can be successfully used as a substrate for developing gas sensors; however, further investigation is needed.

Authors' statement

Research concept and design concept, and design, K.S. and J.K-K.; collection and/or assembly of data, J.K., I.J., M.D., and K.K.; data analysis and interpretation, J.K., J.K-K, and K.S.; writing the article, K.S., J.K-K., and R.K.; critical revision of the article, A.P. and K.S.; final approval of article, A.P., K.S., and J.K-K.

Acknowledgements

This work was supported by the Program of the Republic of Poland – Research Grant MUT project no. UGB 531-000031-W900-22.

References

[1] Leal-Junior, A. *et al.* The role of optical fiber sensors in the new generation of healthcare devices: A review. *Sens. Diagn.* **3**, 1135–1158 (2024). https://doi.org/10.1039/d4sd00032c

[2] Zhao, Y. *et al*. Infrared tapered fiber ring sensor for environmental detection of organic pollutants. *Sens. Actuators B Chem.* **405**, 135361 (2024). https://doi.org/10.1016/j.snb.2024.135361

[3] Bohnert, K., Gabus, P., Kostovic, J. & Brändle, H. Optical fiber sensors for the electric power industry. *Opt. Lasers Eng.* **43**, 511–526 (2005). https://doi.org/10.1016/j.optlaseng.2004.02.008

[4] Wang, P. *et al*. Highly sensitive refractive index and magnetic field sensor based on long-period fiber grating inscribed in tapered optical fiber. *Optik* **289**, 171289 (2023). https://doi.org/10.1016/j.ijleo.2023.171289

[5] Zheng, H. *et al.* High-sensitivity distributed optical fiber sensor for simultaneous hydrostatic pressure and temperature measurement based on birefringent frequency-scanning φ-OTDR. *Opt. Laser Technol.* **175**, 110756 (2024). https://doi.org/10.1016/j.optlastec.2024.110756

[6] Schenato, L., Galtarossa, A., Pasuto, A. & Palmieri, L. Distributed optical fiber pressure sensors. *Opt. Fiber Technol.* **50**, 102239 (2020). https://doi.org/10.1016/j.yofte.2020.102239

[7] Kepak, S., Stolarik, M., Cubik, J., Nedoma, J. & Benes, P. Fiber optic vibration sensor for applications in the field of ground vibrations. *Opt. Laser Technol.* **176**, 111017 (2024). https://doi.org/10.1016/j.optlastec.2024.111017

[8] Chen, G. *et al*. Optical fiber gas sensor with multi-parameter sensing and environmental anti-interference performance. *J. Ind. Inf. Integ.* **38**, 100565 (2024). https://doi.org/10.1016/j.jii.2024.100565

[9] Przybysz, N., Marc, P., Tomaszewska, E., Grobelny, J. & Jaroszewicz, L. R. Pure and Au nanoparticles doped higher alkanes for anoptical fiber temperature threshold sensor. *Proc. SPIE* **10231**, 1023125 (2017). https://doi.org/10.1117/12.2265867

[10] Raghuwanshi, S. K., Kumar, V. & Ansari, M. T. I. Optimizing fiber-optic surface plasmon resonance-based sensors: An exploration of different taper profiles and metal choices for enhanced performance. *Opt. Eng.* **64**, 016101 (2025). https://doi.org/10.1117/1.OE.64.1.016101

[11] Raghuwanshi, S. K., Ansari, M. T. I. & Shadab, A. Analysis of tapered fiber-optic surface plasmon resonance (SPR) bio-sensing probe with the effect of different taper profiles and metal choices. *IEEE Trans. Plasma Sci.* **52**, 295–1303 (2024). https://doi.org/10.1109/TPS.2024.3392672

[12] Raghuwanshi, S. K. Analysis of tapered fiber optic surface plasmon resonance bio-sensor chip with highly perturbed taper profiles. *IEEE Trans. Nanobioscience* **23**, 439–446 (2024). https://doi.org/10.1109/TNB.2024.3376824

[13] Tang, J. *et al.* Optical fiber bio-sensor for phospholipase using liquid crystal. *Biosens. Bioelectron.* **170**, 112547 (2020). https://doi.org/10.1016/j.bios.2020.112547

[14] Moś, J., Stasiewicz, K. A., Matras-Postołek, K. & Jaroszewicz, L. R. Thermo-optical switching effect based on a tapered optical fiber and higher alkanes doped with ZnS:Mn. *Materials* **13**, 5044 (2020). https://doi.org/10.3390/ma13215044

[15] Kiczor, A. & Mergo. P. Comparison of PMMA layers doped with methyl red and CdSe quantum dots for application in fiber optic. *Opto-Electron. Rev.* **32**, e151987 (2024). https://doi.org/10.24425/opelre.2024.151987

[16] Qiu, T., Geng, C., Wu, R. & Tang, X. Metal coating enhancement of optical fiber distributed radiation sensors based on optical frequency domain reflectometry technology. *Opt. Fiber Technol.* **73**, 103063 (2022). https://doi.org/10.1016/j.yofte.2022.103063

[17] Zhao, Y., Li, X., Zhou, X.-G. & Zhang, Y.-N. Review on the graphene based optical fiber chemical and biological sensors. *Sens. Actuators B Chem.* **231**, 324–340 (2016). https://doi.org/10.1016/j.snb.2016.03.026

[18] Chu, R., Tan, Y., Zhou, F. & Liu, Y. Sensitivity-enhanced humidity sensor based on a surface core fiber decorated with graphene oxide. *Sens. Actuators Rep*. **8**, 100207 (2024). https://doi.org/10.1016/j.snr.2024.100207

[19] Eda, G., Fanchini, G. & Chhowalla, M. Large-area ultrathin films of reduced graphene oxide as a transparent and flexible electronic material. *Nat. Nanotechnol.* **3**, 270–274 (2008). https://doi.org/10.1038/nnano.2008.83

[20] Mushahary, N. *et al*. Recent developments on graphene oxide and its composite materials: From fundamentals to applications in biodiesel synthesis, adsorption, photocatalysis, supercapacitors. sensors and antimicrobial activity. *Results Surf. Interfaces* **15**, 100225 (2024). https://doi.org/10.1016/j.rsurfi.2024.100225

[21] Krukowski, P. *et al*. Graphene on quartz modified with rhenium oxide as a semitransparent electrode for organic electronics. *Opto-Electron. Rev.* **30**, e141953 (2022). https://doi.org/10.24425/opelre.2022.141953

[22] Alkhabet, M. M. *et al*. Room temperature operated hydrogen sensor using palladium coated on tapered optical fiber. *Mat. Sci. Eng. B* **287**, 116092 (2023). https://doi.org/10.1016/j.mseb.2022.116092

[23] Zhong, X. *et al*. Recent advances in optical fiber grating sensors for detection of organic substances. *Chem. Eng. J.* **492**, 152260 (2024). https://doi.org/10.1016/j.cej.2024.152260

[24] Kang, X. *et al*. A label-free biosensor for pepsin detection based on graphene oxide functionalized micro-tapered long period fiber grating. *Sens. Actuators Rep*. **5**, 100139 (2023). https://doi.org/10.1016/j.snr.2023.100139

[25] Priya, A. K., Muruganandam, M., Venkatraman, Y. & Sagadevan, S. Recent advances and synergistic interactions in graphene-based polymer nanocomposites for enhanced gas sensing applications. *J. Alloys Compd.* **1008**, 176599 (2024). https://doi.org/10.1016/j.jallcom.2024.176599

[26] Moura, P. C., Pivetta, T. P., Vassilenko, V., Ribeiro, P. A. & Raposo, M. Graphene oxide thin films for detection and quantification of industrially relevant alcohols and acetic acid. *Sensors* **23**, 462 (2023). https://doi.org/10.3390/s23010462

[27] Mandeep, S., Raghuwanshi, S. & Prakash, O. Ultra-sensitive fiber optic gas sensor using graphene oxide coated long period gratings. *IEEE Photonics Technol. Lett.* **31**, 1473 –1476 (2019). https://doi.org/10.1109/LPT.2019.2932764

[28] Yang, Q. *et al*. Highly sensitive and selective sensor probe using glucose oxidase/gold nanoparticles/graphene oxide functionalized tapered optical fiber structure for detection of glucose. *Optik* ***208***, 164536 (2020). https://doi.org/10.1016/j.ijleo.2020.164536

[29] Alkhabet, M. M. *et al*. Palladium/graphene oxide nanocomposite for hydrogen gas sensing applications based on tapered optical fiber. *Materials* **15**, 8167 (2022**)**. https://doi.org/10.3390/ma15228167

[30] Qi, Q. *et al*. A gas-liquid sensor functionalized with graphene-oxide on chalcogenide tapered fiber by chemical etching. *J. Light. Technol.* **39**, 6976–6984 (2021). https://doi.org/10.1109/JLT.2021.3104407

[31] Yu, C. *et al*. Miniature fiber-optic NH3 gas sensor based on Pt nanoparticle-incorporated graphene oxide. *Sens. Actuators B Chem*. **244**, 107–113 (2017). https://doi.org/10.1016/j.snb.2016.12.126

[32] Xiao, Y. *et al.* Reduced graphene oxide for fiber optic toluene gas sensing. *Opt. Exp.* **25**, 28290–28302 (2016). https://doi.org/10.1364/OE.24.028290

[33] Stasiewicz, K. A., Jakubowska I., Korec, J. & Matras-Postołek, K. Modification of higher alkanes by nanoparticles to control light propagation in tapered fibers. *Micromachines* **11**, 1006 (2020). https://doi.org/10.3390/mi11111006

[34] Brambilla G. Optical fiber nanowires and microwires: A review. *J. Opt.* **12**, 043001 (2010). https://doi.org/10.1088/2040-8978/12/4/043001

[35] Birks, T. A. & Li, Y. W. The shape of fiber tapers. *J. Light. Technol.* **10**, 432–438 (1992). https://doi.org/10.1109/50.134196

[36] Stasiewicz, K. A. *et al.* The biopolymer active surface for optical fiber sensors. *Polymers* **16**, 2114 (2024). https://doi.org/10.3390/polym16152114

[37] Jung, Y., Brambilla, G. & Richardson, D. J. Broadband single-mode operation of standard optical fibers by using a sub-wavelength

optical wire filter. *Opt. Exp.* **16**, 14661–14667 (2008). https://doi.org/10.1364/OE.16.014661

[38] Kowiorski, K. *et al*. Compositing graphene oxide with carbon fibers enables improved dynamical thermomechanical behavior of papers produced at a large scale. *Carbon* **206**, 26–36 (2023). https://doi.org/10.1016/j.carbon.2023.02.009

[39] Djas, M. *et al*. Flake graphene as an innovative additive to grease with improved tribological properties. *Materials* **15**, 7775 (2022). https://doi.org/10.3390/ma15217775

[40] Stasiewicz, K. A., Jakubowska, I., Moś, J., Kosturek, R. & Kowiorski, K. In-line gas sensor based on the optical fiber taper technology with a graphene oxide layer. *Electronics* **12**, 830 (2023). https://doi.org/10.3390/electronics12040830